Active Suspension Modelling and LQR Controller Design for a High-Speed Train Under Continuous Road Disturbance and Parameter Uncertainty

Mehmet KARAHAN
TOBB University of Economics and Technology, 43 Sogutozu Street, Ankara, 06510, Turkiye
mehmetkarahan@etu.edu.tr

Abstract: High-speed trains provide a faster and much cheaper transport in comparison with air transport for distances shorter than 640 km. Also, in contrast with road transport, they feature a much lower accident rate and a higher passenger and freight capacity, they are more durable, take up less space, and produce fewer carbon emissions. Therefore, high-speed trains are an attractive transportation option. However, as high-speed trains travel at speeds of at least 200 km/h, even a small bump on the railway track can cause significant vibrations which can lead to wheel slippage, jeopardizing the passenger comfort and safety. Therefore, high-speed trains require an advanced suspension system. This paper proposes an active suspension system with an LQR controller for a high-speed train. The designed suspension system was tested under continuous road disturbance and parameter uncertainty and a comparative robustness analysis was conducted involving a conventional passive suspension system. Simulations related to the actuator force, sprung mass acceleration, suspension travel, wheel deflection, and body displacements were performed for both suspension systems. In this context, the time responses for both suspension systems were obtained and compared. The analysis revealed that the LQR-controlled active suspension achieved a shorter rise time and settling time and featured lower oscillations. This demonstrates that the proposed system provides passengers with a more comfortable and safer journey.

Keywords: Active suspension, Passive suspension, LQR control, Full-state feedback, High-speed train, Disturbance, Robustness, Ride comfort.

1. Introduction

Trains that can travel at least at 250 km/h on newly constructed lines or 200 km/h on upgraded lines are defined as high-speed trains (Garmendia et al., 2012). High-speed trains offer significant transportation advantages. High-speed trains reduce vehicle traffic in city centers, leaving more walkable space for pedestrians (Pope, 2023). For distances shorter than 400 miles, high-speed trains transport passengers from city center to city center in the same amount of time and at a much lower cost than air transport (Dalla Chiara et al., 2017). A 2018 study in the US (United States) found that traffic congestion causes an annual economic loss of $87 billion (Afrin & Yodo, 2020). The expansion of the high-speed train network prevents economic losses by reducing traffic congestion (Li et al., 2020). Electric high-speed trains reduce the dependence on fossil fuels and prevent environmental pollution (Pomykala & Szelag, 2022). Also, high-speed trains offer a much safer journey in comparison with road transport (Wu & Martin, 2022). Certain studies conducted in the US between 2007 and 2023 calculated the fatality rates per 100,000 passenger miles by transportation method. In 2023, there were 0.52 fatalities per 100,000 passenger miles in road transport, while this rate was only 0.02 for rail transport (National Safety Council, 2025). These statistics reveal that rail transport is 26 times safer than road transport. Furthermore, rail transport has a significantly greater passenger and freight capacity than road transport. A single-line high-speed train can carry 20,000 passengers per hour. This number is equivalent to the hourly capacity of a 10-lane highway and two airports (US High Speed Railway Association, 2025). A standard single-track railway can carry 335,000 tons of freight per km per day, while a four-lane highway can carry 150,000 tons per km per day (Rodrigue, 2024).

Further on, track irregularities on the railway can cause vibrations during travel. These vibrations can be more dangerous at higher speeds. The possible track irregularities encountered on the railway are shown in Figure 1.

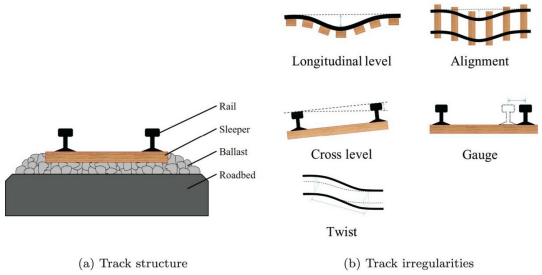

Figure 1. Track irregularities (Tsunashima & Hirose, 2022)

High-speed trains travel at speeds between 200 and 350 km/h. A small bump on the railway track that might not cause a jolt for a train traveling at 100 km/h can cause a significant jolt for a high-

https://doi.org/10.24846/v35i2y202605

speed train. High speed means less time to recover from a wheel slip or imbalance. A high-speed train requires a high-quality suspension system to ensure passengers can enjoy their drinks, work on their laptops, or sleep comfortably without any jolting.

El Amraoui & Mesghouni (2014) optimized a train traffic scheduling problem under traveling time uncertainty. Lee et al. (2013) designed a breaking resistor and carried out its heat analysis simulation for a high-speed train. Zhao & Liu (2025) proposed an operational risk prevention and control model for a high-speed train.

Passive, semi-active and active suspensions can be used in high-speed trains. Passive suspension systems do not have actuators and therefore do not have controllers. Passive suspensions are low-cost, classic systems consisting of springs and dampers. Due to the passive suspension's limited ability to isolate vibration, high-speed trains with passive suspension cannot adapt to track excitations and operating modes. To address this issue, implementing active control to the suspension system is a viable way of enhancing the operational compatibility of high-speed trains on different types of tracks (Wu et al., 2022). Semi-active suspension systems determine the damping constants or spring coefficient according to changing rail conditions, providing a more comfortable ride than passive suspensions with fixed damping coefficients (Chen et al., 2025). On the other hand, active suspensions include an actuator and controller. This allows them to quickly adjust the suspension's softness to changing road conditions. They offer greater comfort than other suspension systems, especially during hard acceleration and hard braking (Nguyen, 2021).

Nguyen et al. (2008) designed a passive suspension system for a railway vehicle. They used norm optimization to obtain optimal parameters of springs and dampers of the railway vehicle. Wu et al. (2024) designed a semi-active suspension based on a magnetorheological elastomer to reduce the lateral resonance for a high-speed train. Gao et al. (2021) designed a semi-active suspension system for a high-speed train that would reduce train body vibration under unsteady aerodynamic loads and random wind speeds. Hua et al. (2022) proposed a semi-active suspension system with a magnetorheological (MR) damper parallel to a magnetic negative stiffness unit to enhance the ride comfort in high-speed trains. Zhang et al. (2024) proposed an active suspension with a sliding mode controller to reduce the impact of strong side winds on high-speed trains traveling on mountainous roads. This reduced the risk of derailment by reducing the wheel load for the high-speed trains. They compared their active suspension with a passive suspension and the former achieved superior results.

This study proposes an active suspension with a full-state feedback LQR controller for a high-speed train. Firstly, the designed LQR-controlled active suspension was subjected to a continuous road disturbance with an amplitude of 0.1 m and a period of 6 seconds. This resulted in a much more comprehensive robustness test in comparison with suspension systems tested under a single, instantaneous disturbance. Secondly, simulations were performed under 20% parameter uncertainty and continuous road disturbance. To demonstrate the superiority of the designed LQR-controlled active suspension, a comparative analysis was conducted including a conventional passive suspension system. Time response data for the two suspension systems was obtained and compared. It was proven that the LQR-controlled active suspension exhibited significantly lower oscillations, a shorter rise time, and a shorter settling time. Furthermore, the RMS values for the designed suspension systems were obtained, which were in accordance with international standards. The simulations demonstrated that the LQR-controlled active suspension was more robust, providing passengers with a safer and more comfortable ride.

The remainder of this paper is structured as follows. Section 2 explains the active and passive suspension models. Section 3 describes the full-state feedback LQR controller, while Section 4 presents the simulations which were carried out. Finally, Section 5 sets forth the conclusion of this paper.

2. Modelling of the Suspension

This section describes suspension models and it includes the equations used for both suspensions. Passive suspensions do not include a controller, so there is no actuator control force applied, and they have a simpler mechanism. Active suspensions, on the other hand, have a more complex structure due to the presence of an actuator and a controller. The mass of a railway vehicle includes two main components: the train's mass, namely the sprung mass, and the bogie's mass, namely the unsprung mass. A bogie is the undercarriage used in railway vehicles. The bogie contains the axle, wheels,

suspension systems, and brake systems. Figure 2 shows the suspension schematics.

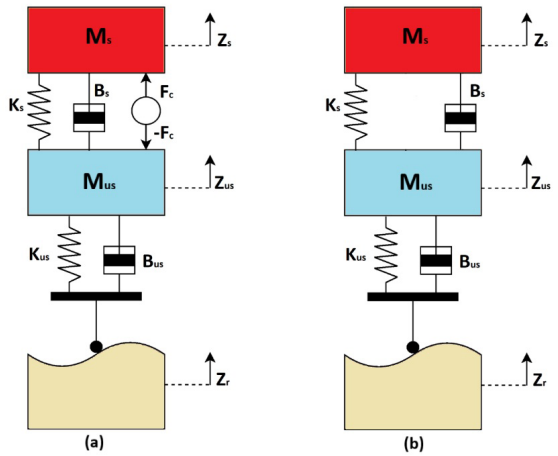

Figure 2. Active (a) and passive (b) suspension (Karahan, 2025)

The description of the suspension parameters is included in Table 1.

Table 1. Description of the suspension parameters

Symbol	Description
M_s	Sprung mass
M_{us}	Unsprung mass
Z_s	Displacement of sprung mass
Z_{us}	Displacement of unsprung mass
B_s	Damping coefficient of sprung mass
B_{us}	Damping coefficient of unsprung mass
K_s	Spring coefficient of sprung mass
K_{us}	Spring coefficient of unsprung mass
F_c	Actuator control force
Z_r	Excitation due to railway disturbance

The suspension coefficients are rendered in Table 2.

Table 2. Suspension coefficients

Symbol	Value
M_s	5333 kg
M_{us}	906.5 kg
B_s	20000 s/m
B_{us}	40000 s/m
K_s	430000 N/m
K_{us}	2440000 N/m

2.1 Equations of the Suspensions

The equations of motion for the active and passive suspensions are obtained using Newton's 2nd law, given in equation (1):

$$F = ma \tag{1}$$

Rewriting equation (1) to express acceleration yields equation (2):

$$a = \frac{F}{m} \tag{2}$$

Using Newton's law, the active suspension's motion equation is derived as given in equation (3):

$$M_s\ddot{Z}_s = B_s\dot{Z}_{us} - B_s\dot{Z}_s - K_s(Z_s - Z_{us}) + F_c \tag{3}$$

Rewriting equation (3) to express the acceleration of the sprung mass yields equation (4):

$$\ddot{Z}_s = \frac{B_s\dot{Z}_{us}}{M_s} - \frac{B_s\dot{Z}_s}{M_s} - \frac{K_s(Z_s - Z_{us})}{M_s} + \frac{1}{M_s}F_c \tag{4}$$

Equation (5) gives the forces on the unsprung mass:

$$\begin{aligned} M_{us}\ddot{Z}_{us} &= -B_s\dot{Z}_{us} - B_{us}\dot{Z}_{us} + B_s\dot{Z}_s + B_{us}\dot{Z}_r \\ &-K_s(Z_{us} - Z_s) - K_{us}(Z_{us} - Z_r) - F_c \end{aligned} \tag{5}$$

Dividing the two sides of equation (5) by M_{us} gives the acceleration of the unsprung mass in equation (6):

$$\begin{aligned} \ddot{Z}_{us} &= -\frac{B_s\dot{Z}_{us}}{M_{us}} - \frac{B_{us}\dot{Z}_{us}}{M_{us}} + \frac{B_s\dot{Z}_s}{M_{us}} + \frac{B_{us}\dot{Z}_r}{M_{us}} \\ &-\frac{K_s(Z_{us} - Z_s)}{M_{us}} - \frac{K_{us}(Z_{us} - Z_r)}{M_{us}} - \frac{1}{M_{us}}F_c \end{aligned} \tag{6}$$

2.2 State Space

The state variables of active suspension are represented in this subsection. The general representation of a state space is as given in equation (7):

$$\begin{aligned} \dot{x} &= Ax + Bu \\ y &= Cx + Du \end{aligned} \tag{7}$$

The description of the state variables is included in Table 3.

Table 3. Description of the state variables

Variable	Description
x	State variables vector
$\dot{x}$	Derivative of the state variables vector
u	Input vector
y	Output vector
A	System matrix
B	Input matrix
C	Output matrix
D	Feedforward matrix

The state-space variables of the active suspension are defined in equation (8). The state space is constructed by using the previously obtained equations and the state variables in equation (8). In equation (8), $Z_s - Z_{us}$ denotes the suspension travel. $\dot{Z}_s$ symbolizes the speed of the train body, $Z_{us} - Z_r$ is the wheel deflection and $\dot{Z}_{us}$ is the vertical speed of the wheel.

$$\begin{Bmatrix} X_1 = Z_s - Z_{us} \\ X_2 = \dot{Z}_s \\ X_3 = Z_{us} - Z_r \\ X_4 = \dot{Z}_{us} \end{Bmatrix} \tag{8}$$

Using the above equations, the state space of the active suspension could be presented as in equations (9) and (10):

$$\begin{bmatrix} \dot{x}_1 \\ \dot{x}_2 \\ \dot{x}_3 \\ \dot{x}_4 \end{bmatrix} = \begin{bmatrix} 0 & 1 & 0 & -1 \\ -\frac{K_s}{M_s} & -\frac{B_s}{M_s} & 0 & \frac{B_s}{M_s} \\ 0 & 0 & 0 & 1 \\ \frac{K_s}{M_{us}} & \frac{B_s}{M_{us}} & -\frac{K_{us}}{M_{us}} & -\frac{B_s + B_{us}}{M_{us}} \end{bmatrix} \begin{bmatrix} x_1 \\ x_2 \\ x_3 \\ x_4 \end{bmatrix} + \begin{bmatrix} 0 & 0 \\ 0 & \frac{1}{M_s} \\ -1 & 0 \\ \frac{B_{us}}{M_{us}} & -\frac{1}{M_{us}} \end{bmatrix} \begin{bmatrix} \dot{Z}_r \\ F_c \end{bmatrix} \tag{9}$$

$$\begin{bmatrix} y_1 \\ y_2 \end{bmatrix} = \begin{bmatrix} 1 & 0 & 0 & 0 \\ -\frac{K_s}{M_s} & -\frac{B_s}{M_s} & 0 & \frac{B_s}{M_s} \end{bmatrix} \begin{bmatrix} x_1 \\ x_2 \\ x_3 \\ x_4 \end{bmatrix} + \begin{bmatrix} 0 & 0 \\ 0 & \frac{1}{M_s} \end{bmatrix} \begin{bmatrix} \dot{Z}_r \\ F_c \end{bmatrix} \tag{10}$$

The matrices A, B, C, and D are as shown in the following equations:

$$A = \begin{bmatrix} 0 & 1 & 0 & -1 \\ -\frac{K_s}{M_s} & -\frac{B_s}{M_s} & 0 & \frac{B_s}{M_s} \\ 0 & 0 & 0 & 1 \\ \frac{K_s}{M_{us}} & \frac{B_s}{M_{us}} & -\frac{K_{us}}{M_{us}} & -\frac{B_s + B_{us}}{M_{us}} \end{bmatrix} \tag{11}$$

$$B = \begin{bmatrix} 0 & 0 \\ 0 & \frac{1}{M_s} \\ -1 & 0 \\ \frac{B_{us}}{M_{us}} & -\frac{1}{M_{us}} \end{bmatrix} \tag{12}$$

$$C = \begin{bmatrix} 1 & 0 & 0 & 0 \\ -\frac{K_s}{M_s} & -\frac{B_s}{M_s} & 0 & \frac{B_s}{M_s} \end{bmatrix} \tag{13}$$

$$D = \begin{bmatrix} 0 & 0 \\ 0 & \frac{1}{M_s} \end{bmatrix} \tag{14}$$

3. Full State Feedback LQR

In this section, the full state feedback LQR control design is explained. This approach is an ideal way for finding the intended pole positions of a closed-loop system. It ensures that all state variables are known to the controller and available for feedback. A state-space matrix is a system in which each state variable is fed back to the input u via a gain K, symbolized by a feedback vector that could be determined in order to obtain the desired closed-loop poles (Karboua et al., 2025). The input u is expressed in equation (15):

$$u = -Kx \tag{15}$$

Substituting equation (15) into equation (11) gives the state space for the closed-loop system:

$$\dot{x} = Ax - BKx \tag{16}$$

A full-state feedback control scheme is given in Figure 3.

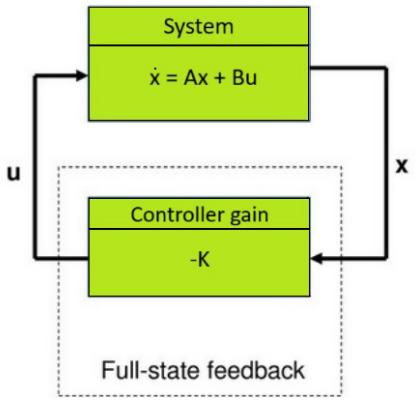

Figure 3. Full-state feedback control

The LQR approach is a type of state feedback control that allows the controller gain K to be

systematically determined. The LQR control method is used in linear MIMO (multiple-input multiple-output) systems. The advantage of the LQR controller lies in the fact that the factors affecting the performance index can be weighted based on the desired outcome. The aim of the LQR control design presented in this study is to increase the ride comfort by improving the rail handling ability. The main function of the LQR control is to minimize the cost function *J*, given as the performance index in equation (17), and to calculate the optimal gain K (Rajendran et al., 2025).

$$J = \frac{1}{2}\int_0^t (x^t Qx + u^t Ru)dt \tag{17}$$

In equation (17), x^t presents the state vector and u^t symbolizes the control input. The LQR controller is constructed by achieving the appropriate *Q* and *R* values to minimize the *J* function. In this study, the Q matrix is a positive diagonal matrix, and R represents a positive number. The LQR controller is adjusted by changing the *Q* matrix in order to penalize a poor performance or by changing the *R* matrix in order to penalize actuator effort until the desired closed-loop response is achieved. Based on equation (14), the feedback regulator and responsive performance index are obtained as in equation (18):

$$F_c = -Kx \tag{18}$$

The *Q* matrix is the weight matrix of the system states. The *R* matrix is the weight matrix of the control input. Since the system has four states, the *Q* matrix is a 4x4 matrix and since the system has a single control input, that is u, the *R* matrix is a 1x1 matrix. Relatively important performance metrics that deserve more attention are those related to the suspension motion and train body acceleration. The *Q* and *R* matrices, determined for minimizing the cost function J, are given in equations (19) and (20):

$$Q = \begin{bmatrix} 1760\times10^6 & 0 & 0 & 0 \\ 0 & 11.6\times10^6 & 0 & 0 \\ 0 & 0 & 1 & 0 \\ 0 & 0 & 0 & 1 \end{bmatrix} \tag{19}$$

$$R = [0.01] \tag{20}$$

The gain value *K* in equation (21) is obtained by introducing the *A* and *B* matrices in the state space and the *Q* and *R* weight matrices as inputs to the LQR function in MATLAB:

$$K = [1.708\times10^5 \quad 0.364\times10^5 \quad 0.776\times10^5 \quad 0.005\times10^5] \tag{21}$$

4. Simulations

Simulations of active and passive suspensions modeled with Simulink were performed under a continuous road disturbance with an amplitude of 0.1 m and a period of 6 seconds, and a parameter uncertainty of +20%. The actuator force, suspension travel, sprung mass acceleration, wheel deflection, and body displacements were simulated. The simulations were performed for 10 seconds. Time response data for the active and passive suspension was obtained and analyzed. The rise time is the time required to reach 90% of the reference line. The overshoot value is a numerical value calculated in m or m/s^2. The settling time is the time required to settle within ± 5% of the given reference line. The Simulink model depicting the active suspension, passive suspension, and rail track disturbance is shown in Figure 4.

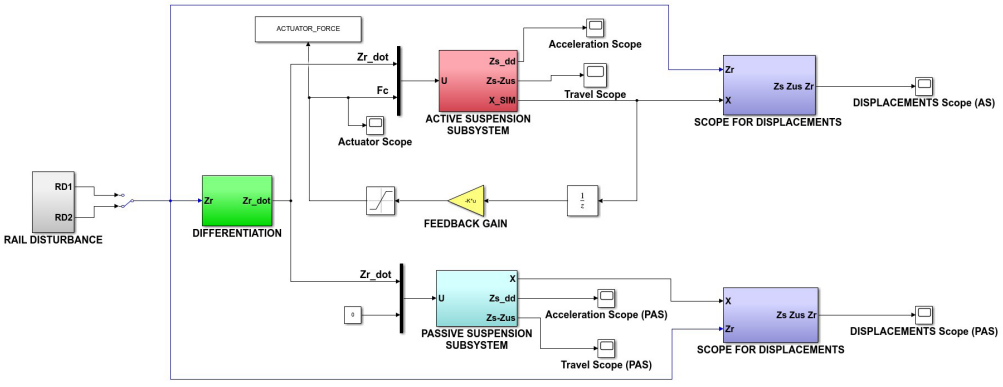

Figure 4. Active suspension, passive suspension and rail track disturbance

4.1 Simulations Under Continuous Road Disturbance

The actuator force of the active suspension when a continuous road disturbance is applied in the form of a square wave is shown in Figure 5. Since the passive suspension does not include an actuator, an actuator force simulation has not been performed for it.

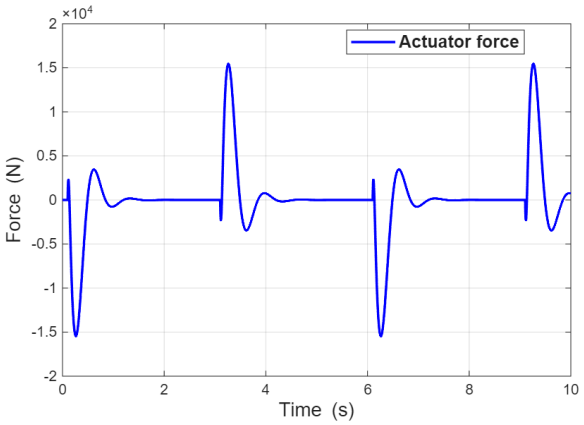

Figure 5. Actuator force simulation for the active suspension under continuous road disturbance

The time response data for the actuator force is included in Table 4. The actuator force reaches 90% of the reference value in 0.466 seconds. The overshoot value is 15450 N. When a rail disturbance is applied to the railway vehicle, the active suspension actuator applies a force of 15450 N to balance the system. The active suspension actuator reaches within ± 5% of the reference value in 0.972 seconds.

Table 4. Time response data for the actuator force of the active suspension under continuous road disturbance

Time response	Value
Rise time	0.466 s
Overshoot	15450 N
Settling time	0.972 s

The sprung mass acceleration simulation under continuous road disturbance is depicted in Figure 6. The red line in the graph indicates the acceleration of the active suspension, while the dashed blue line indicates the acceleration of the passive suspension. The vertical axis indicates the acceleration value, and its unit is m/s². The horizontal axis indicates the time, expressed is seconds.

The time response data for Figure 6 is given in Table 5. By examining the data in the table, it can be noticed that active suspension has a shorter rise time than passive suspension. To that, the overshoot of the active suspension is slightly greater than that of the passive suspension. Further on, the active suspension has a much shorter settling time in comparison with the passive suspension. Finally, the active suspension reaches within ± 5% of the reference value in approximately one-third of the settling time obtained by the passive suspension. The passive suspension oscillates excessively and, therefore, it needs a longer settling time.

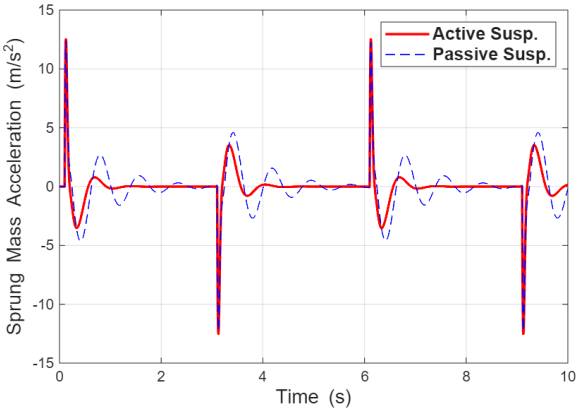

Figure 6. Sprung mass acceleration simulation under continuous road disturbance

The RMS value can be calculated by multiplying the peak-to-peak amplitude by 0.35355. According to international standards such as UIC 515-1 and TSI RST HS 232, high-speed trains typically use a peak lateral acceleration threshold of 0.8g (7.85 m/s²) as a safety limit for detecting oscillation instability. According to the Hunting Stability Criterion, the acceleration of the vehicle body in high-speed trains should not frequently exceed 0.8g (Liang et al., 2024). Table 5 also shows the obtained RMS values for the active and passive suspension, which are in accordance with the UIC 515-1 and TSI RST HS 232 standards. The acceleration value for the active suspension is 5.67 m/s², and the acceleration value for the passive suspension is 6 m/s². As such, the active suspension is safer and more comfortable due to its lower acceleration.

Table 5. Time response data for the sprung mass acceleration under continuous road disturbance

Suspension	Rise time (s)	Overshoot (m/s²)	Settling time (s)	RMS (m/s²)
Active	0.491 s	12.52 m/s²	0.525 s	5.67 m/s²
Passive	0.587 s	12.35 m/s²	1.673 s	6.00 m/s²

Further on, the suspension travel simulation under continuous road disturbance is represented in Figure 7.

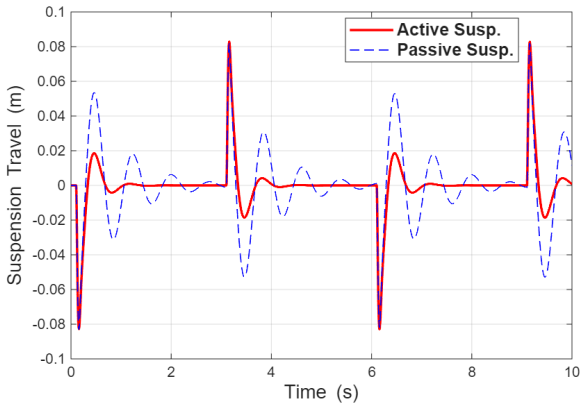

Figure 7. Suspension travel simulation under continuous road disturbance

The time response data for Figure 7 is included in Table 6. As regards the rise time in the simulation, the active suspension appears to have a longer rise time than the passive suspension. As the overshoot is concerned, the active suspension has a higher overshoot. However, when examining the settling time, it is clear that the active suspension has a much shorter settling time: the active suspension has a settling time of 0.815 s, while the passive suspension has a longer settling time of 2.106 s and oscillates for a longer period.

Table 6. Time response data for the suspension travel under continuous road disturbance

Suspension	Rise time (s)	Overshoot (m)	Settling time (s)
Active	0.309 s	0.0827 m	0.815 s
Passive	0.277 s	0.0817 m	2.106 s

The wheel deflection simulation under continuous road disturbance is illustrated in Figure 8. The red line in the graph represents the wheel deflection of the active suspension, while the dashed blue line represents the wheel deflection of the passive suspension. The vertical axis represents the wheel deflection expressed in meters, and the horizontal axis represents time expressed in seconds.

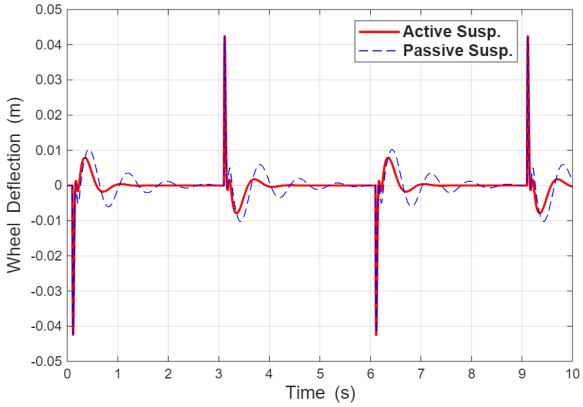

Figure 8. Wheel deflection simulation under continuous road disturbance

The time response data for wheel deflection under continuous road disturbance is rendered in Table 7. For the wheel deflection simulation, the rise times of the two suspensions are the same. While the overshoot values are very similar, the active suspension overshoots 0.0003 m more than the passive suspension. The active suspension's settling time is 0.52 s, while the passive suspension's settling time is 1.317 s. The active suspension reaches within ± 5% of the reference value in 40% of the passive suspension's settling time, exhibiting lower oscillations.

Table 7. Time response data for the wheel deflection under continuous road disturbance

Suspension	Rise time (s)	Overshoot (m)	Settling time (s)
Active	0.152 s	0.0424 m	0.52 s
Passive	0.152 s	0.0421 m	1.317 s

The time response for body displacements for the passive suspension under continuous road disturbance is presented in Figure 9. The red line in the graph represents the sprung mass, the blue line symbolizes the unsprung mass, and the green line represents the track profile. The body displacements for the passive suspension are expressed in meters, and the time in seconds.

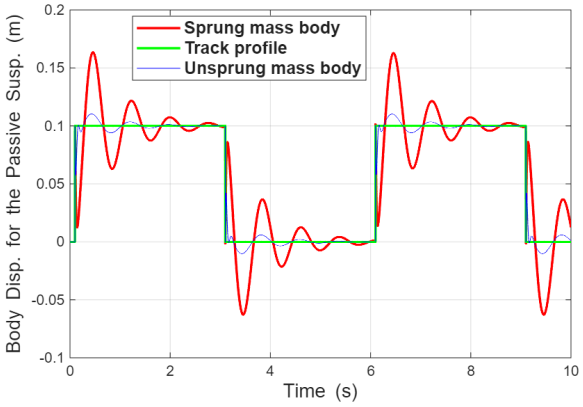

Figure 9. Body displacements for the passive suspension under continuous road disturbance

The time response data for Figure 9 is given in Table 8. By analyzing the data in Table 8 it can be noted that the sprung mass has a longer rise time than the unsprung mass. The sprung mass also exhibits a higher overshoot and takes longer to settle.

Table 8. Body displacements for the passive suspension under continuous road disturbance

Body displacement	Rise time (s)	Overshoot (m)	Settling time (s)
Sprung mass	0.272 s	0.163 m	2.09 s
Unsprung mass	0.145 s	0.110 m	0.91 s

The time response for body displacements for the active suspension under continuous road disturbance is presented in Figure 10. The red line in the graph represents the sprung mass, the blue line represents the unsprung mass, and the green line represents the track profile. The body displacements for the active suspension is expressed in meters, and the time in seconds.

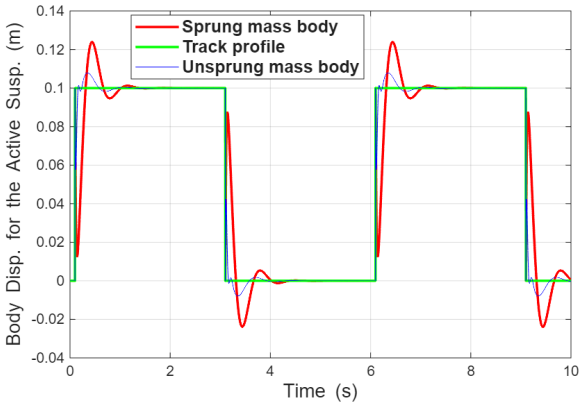

Figure 10. Body displacements for the active suspension under continuous road disturbance

The time response data for the simulation related to body displacements for the sprung mass and unsprung mass of the active suspension is given in Table 9. By analyzing the data in Table 9, it can be noted that the rise time of the sprung mass is twice the rise time of the unsprung mass. The overshoot value of the sprung mass is also higher than the overshoot value of the unsprung mass. Further on, the settling time of the sprung mass is approximately twice the settling time of the unsprung mass.

Table 9. Body displacements for the active suspension under continuous road disturbance

Body displacement	Rise time (s)	Overshoot (m)	Settling time (s)
Sprung mass	0.290 s	0.124 m	0.841 s
Unsprung mass	0.145 s	0.108 m	0.456 s

By comparing the body displacement data for the active suspension in Table 9 with the body displacement data for the passive suspension in Table 8, the results are as follows. The body displacement of the sprung mass in the active suspension has a longer rise time than the body displacement of the sprung mass in the passive suspension. As the rise time of the unsprung masses is concerned, it is the same for both suspension systems. Further on, for the active suspension, the overshoot values of both the sprung and unsprung masses are lower than those in the passive suspension system. Finally, the settling time values for both the sprung and unsprung masses in the active suspension are significantly lower than those in the passive suspension.

It is clear that the body displacement overshoot values and settling time values for the active suspension are lower than those in the passive suspension. This demonstrates that the active suspension offers a more comfortable and stable journey.

4.2 Simulations Under Parameter Uncertainty and Continuous Road Disturbance

In this section, simulations were repeated by applying a +20% parameter uncertainty to the M_s, M_{us}, K_s, K_{us}, B_s, and B_{us} values. The actuator force simulation for the active suspension performed under parameter uncertainty and continuous road disturbance is given in Figure 11.

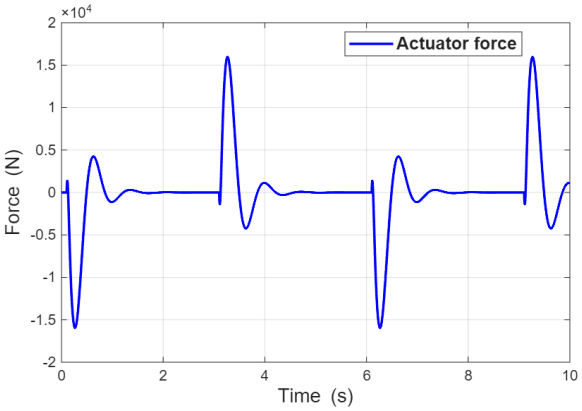

Figure 11. Actuator force simulation under parameter uncertainty and continuous road disturbance

The time response data for the actuator force under parameter uncertainty and continuous road disturbance is included in Table 10.

Table 10. Time response data for the actuator force of the active suspension under parameter uncertainty and continuous road disturbance

Time response	Value
Rise time	0.47 s
Overshoot	15952 N
Settling time	1.073 s

By examining the data in Table 10, it can be seen that the rise time has been slightly extended due to the effect of parameter uncertainty. There is also a slight increase in the value of the overshoot and settling time.

Figure 12 shows the sprung mass acceleration simulation under parameter uncertainty and continuous road disturbance.

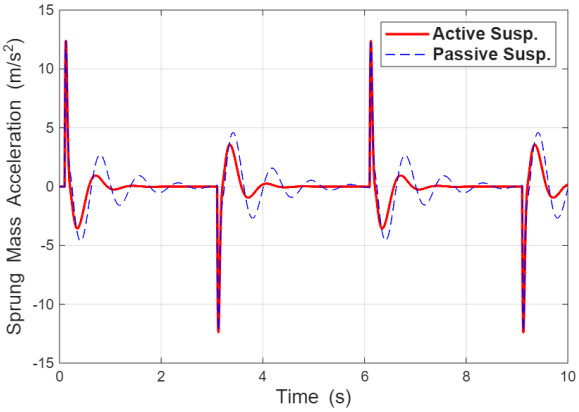

Figure 12. Sprung mass acceleration simulation under parameter uncertainty and continuous road disturbance

Table 11 includes the time response data for the sprung mass acceleration simulation under parameter uncertainty. The active suspension under parameter uncertainty features a longer rise time, a lower overshoot, a longer settling time, and a lower RMS value in comparison with the active suspension under normal conditions. The applied parameter uncertainty led to longer but smoother responses for the active suspension. The time response data for the passive suspension under parameter uncertainty and continuous road disturbance is the same as in the previous simulation, which did not involve parameter uncertainty. Since the passive suspension is not adaptable to parameter uncertainty, its responses were identical.

Table 11. Time response data for the sprung mass acceleration under parameter uncertainty and continuous road disturbance

Suspension	Rise time (s)	Overshoot (m/s²)	Settling time (s)	RMS (m/s²)
Active	0.508 s	12.36 m/s²	0.815 s	5.62m/s²
Passive	0.587 s	12.35 m/s²	1.673 s	6.00 m/s²

Figure 13 illustrates the suspension travel simulation under parameter uncertainty and continuous road disturbance.

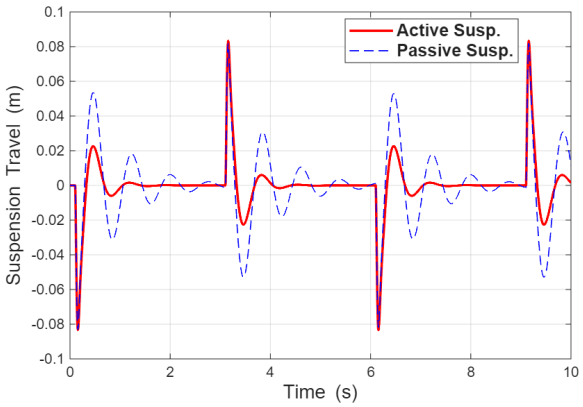

Figure 13. Suspension travel simulation under parameter uncertainty and continuous road disturbance

Table 12 renders the time response data for the suspension travel simulation under parameter uncertainty. In this case, the rise time for the active suspension decreased by 0.04 seconds in comparison with the previous simulation, which did not involve parameter uncertainty. The overshoot value decreased by 0.0005 m. The settling time, however, increased by 0.104 seconds. With regard to the passive suspension, under parameter uncertainty its rise time remained the same as in the previous simulation, which did not involve parameter uncertainty. The overshoot value increased by 0.0012 m, while the settling time decreased by 0.003 seconds.

Table 12. Time response data for the suspension travel under parameter uncertainty and continuous road disturbance

Suspension	Rise time (s)	Overshoot (m)	Settling time (s)
Active	0.305 s	0.0832 m	0.919 s
Passive	0.277 s	0.0829 m	2.103 s

Figure 14 gives the wheel deflection simulation under parameter uncertainty and continuous road disturbance.

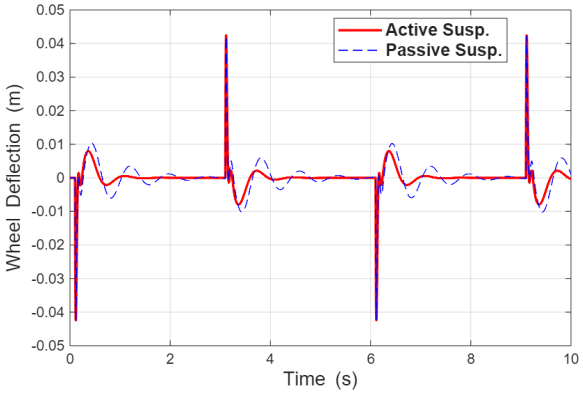

Figure 14. Wheel deflection simulation under parameter uncertainty and continuous road disturbance

Table 13 includes the time response data for the wheel deflection under parameter uncertainty and continuous road disturbance. Under parameter uncertainty, the rise time and overshoot values for the active suspension are the same as in the previous simulation, which did not involve parameter uncertainty, while the settling time is 0.24 seconds longer. With regard to the passive suspension, under parameter uncertainty its rise time and settling time remained the same in comparison with the previous simulation, which did not involve parameter uncertainty, but the settling time has increased by 0.002 m.

Table 13. Time response data for the wheel deflection under parameter uncertainty and continuous road disturbance

Suspension	Rise time (s)	Overshoot (m)	Settling time (s)
Active	0.152 s	0.0424 m	0.76 s
Passive	0.152 s	0.0423 m	1.317 s

Figure 15 depicts the body displacements for the passive suspension under parameter uncertainty and continuous road disturbance.

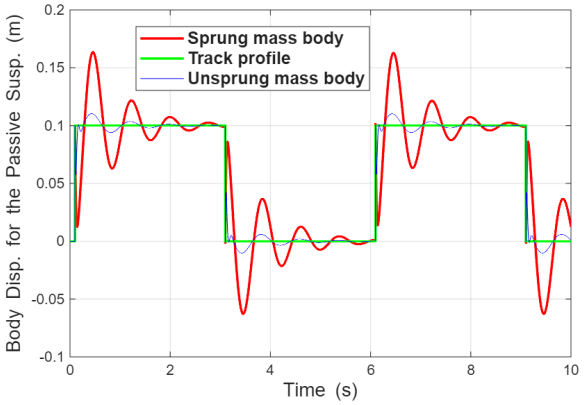

Figure 15. Body displacements for the passive suspension under parameter uncertainty and continuous road disturbance

Table 14 shows the time response of the body displacements for the passive suspension under parameter uncertainty and continuous road disturbance. In this case, the rise time, overshoot, and settling time values for the sprung mass and unsprung mass body displacements for the passive suspension are the same as in the previous simulation, which did not involve parameter uncertainty. Due to the simple structure of the passive suspension and its inability to adapt to track excitations and different operating modes, it is normal for it to exhibit the same responses under parameter uncertainty and continuous road disturbance.

Table 14. Body displacements for the passive suspension under parameter uncertainty and continuous road disturbance

Body displacement	Rise time (s)	Overshoot (m)	Settling time (s)
Sprung mass	0.272 s	0.163 m	2.09 s
Unsprung mass	0.145 s	0.110 m	0.91 s

Figure 16 shows the body displacements for the active suspension under parameter uncertainty and continuous road disturbance.

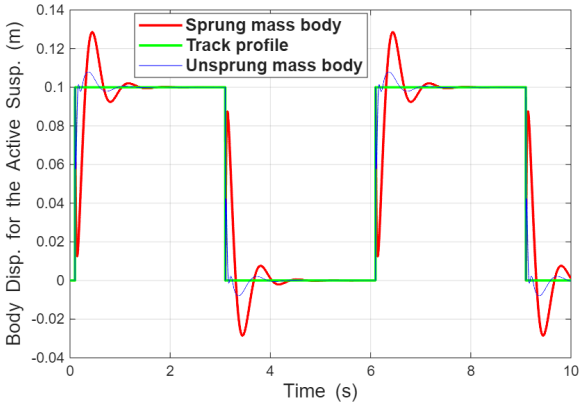

Figure 16. Body displacements for the active suspension under parameter uncertainty and continuous road disturbance

Table 15 renders the time response of the sprung mass body displacements for the active suspension under parameter uncertainty and continuous road disturbance. In this case, it can be noticed that the rise time is shorter by 0.002 s, the overshoot is higher by 0.004 m, and the settling time is longer by 0.075 s in comparison with the previous simulation, which did not involve parameter uncertainty. So, due to parameter uncertainty, a faster rise time, a higher overshoot value, and a longer settling time are noted. However, since the increments are small, there is no significant change that would affect passenger comfort. Further on, as regards the unsprung mass body displacement simulation for the active suspension under parameter uncertainty, it is observed that the rise time and overshoot remain the same, while the settling time increases by 0.016 s. So, it can be said that the unsprung mass is less affected by parameter uncertainty.

Table 15. Body displacements for the active suspension under parameter uncertainty and continuous road disturbance

Body displacement	Rise time (s)	Overshoot (m)	Settling time (s)
Sprung mass	0.288 s	0.128 m	0.916 s
Unsprung mass	0.145 s	0.108 m	0.472 s

5. Conclusion

This research was conducted for modelling of an active suspension system and designing an LQR controller for a high-speed train under continuous road disturbance and a +20% parameter uncertainty. Comparative simulations were carried out for proving the advantages of the proposed active suspension over the conventional passive suspension, involving sprung mass acceleration, suspension travel, wheel deflection, and body displacement. Time response data was obtained for both suspension systems. It was noted that the active suspension with an LQR controller achieved a significantly shorter settling time and featured significantly lower oscillations in comparison with the passive suspension. Also, the obtained RMS values for both the active and passive suspensions comply with international standards and the active suspension enables a more comfortable journey due to its lower RMS values. Parameter uncertainty increased the magnitude of the required actuator force by 42 N for the active suspension. Passive suspension does not include an actuator; therefore, no increased actuator force or controller effort was necessary. The simulations conducted under parameter uncertainty also showed that the active suspension performed better than the passive suspension. Since the passive suspension is a fixed suspension system that does not adapt to changing road conditions, its performance metrics remained largely the same even under parameter uncertainty. Thus, it was confirmed that the proposed active suspension with an LQR controller provides a much more comfortable and safe ride than the conventional passive suspension.

REFERENCES

Afrin, T. & Yodo, N. (2020) A survey of road traffic congestion measures towards a sustainable and resilient transportation system. *Sustainability*. 12(11), Art. ID 4660. https://doi.org/10.3390/su12114660.

Chen, X., Wang, Z., Shi, H. et al. (2025) Review of Agricultural Machinery Seat Semi-Active Suspension Systems for Ride Comfort. *Machines*. 13(3), Art. ID 246. https://doi.org/10.3390/machines13030246.

Dalla Chiara, B., De Franco, D., Coviello, N. et al. (2017) Comparative specific energy consumption between air transport and high-speed rail transport: A practical assessment. *Transportation Research Part D: Transport and Environment*. 52(A), 227-243. https://doi.org/10.1016/j.trd.2017.02.006.

El Amraoui, A. & Mesghouni, K. (2014). Optimization of a train traffic management problem under uncertainties and disruptions. *Studies in Informatics and Control*. 23(4), 313-322. https://doi.org/10.24846/v23i4y201401.

Gao, Z. Y., Tian, B., Wu, D. P. et al. (2021) Study on semi-active control of running stability in the high-speed train under unsteady aerodynamic loads and track excitation. *Vehicle System Dynamics*. 59(1), 101-114. https://doi.org/10.1177/10775463251316913.

Garmendia, M., Ribalaygua, C. & Ureña, J. M. (2012) High speed rail: implication for cities. *Cities*. 29, S26-S31. https://doi.org/10.1016/j.cities.2012.06.005.

Hua, Y., Zhu, S. & Shi, X. (2022) High-performance semiactive secondary suspension of high-speed trains using negative stiffness and magnetorheological dampers. *Vehicle System Dynamics*. 60(7), 2290-2311. https://doi.org/10.1080/00423114.2021.1899251.

Karahan, M. (2025) Modeling and LQR Feedback Control for an Active Suspension of a High-Speed Train. *Mühendislik Bilimleri ve Araştırmaları Dergisi* [*Journal of Engineering Sciences and Researches*]. 7(1), 83-92. https://doi.org/10.46387/bjesr.1639115.

Karboua, D., Toual, B., Mosaad, M. I. et al. (2025) Performance enhancement of PMSM using a hybridizing of nonlinear backstepping control and an optimized linear quadratic regulator. *Energy Exploration & Exploitation*. 43(6), 2637-2664. https://doi.org/10.1177/01445987251353243.

Lee, D.-D., Shim, J.-M., & Hyun, D.-S. (2013). Temperature characteristics analysis of braking resistor for high speed train. *Studies in Informatics and Control*. 22(1), 25-32. https://doi.org/10.24846/v22i1y201303.

Li, Y., Chen, Z. & Wang, P. (2020) Impact of high-speed rail on urban economic efficiency in China. *Transport Policy*. 97, 220-231. https://doi.org/10.1016/j.tranpol.2020.08.001.

Liang, J., Sun, J., Jiang, Y. et al. (2024). Advances and challenges in the hunting instability diagnosis of high-speed trains. *Sensors*. 24(17), Art. ID 5719. https://doi.org/10.3390/s24175719.

National Safety Council (NSC). (2025) *Deaths by Transportation Mode.* https://injuryfacts.nsc.org/home-and-community/safety-topics/deaths-by-transportation-mode/ [Accessed 19th October 2025].

Nguyen, H. C., Sone, A., Iba, D. et al. (2008) Design of passive suspension system of railway vehicles via control theory. *Journal of System Design and Dynamics*. 2(2), 518-527. https://doi.org/10.1299/jsdd.2.518.

Nguyen, T. A. (2021) Improving the Comfort of the Vehicle Based on Using the Active Suspension System Controlled by the Double-Integrated Controller. *Shock and Vibration*. 2021(1), Art. ID 1426003. https://doi.org/10.1155/2021/1426003.

Pomykala, A. & Szelag, A. (2022) Reduction of power consumption and CO_2 emissions as a result of putting into service high-speed trains: Polish case. *Energies*. 15(12), Art. ID 4206. https://doi.org/10.3390/en15124206.

Pope, N. A. (2023) *Unraveling the pedestrian environments of high-speed rail station areas: a comparative case study from Japan and lessons for America's urban walkability*. PhD thesis, University of Texas at Austin. https://doi.org/10.26153/tsw/51436.

Rajendran, A., Jayamani, R., & Kiruban, M. (2025). Optimized LQR Control for Dual-Input Boost Converter in Hybrid PV-Wind System for Remote Telephony Applications. *Studies in Informatics and Control*. 34(4), 53-62. https://doi.org/10.24846/v34i4y202505.

Rodrigue, J.-P. (2024) Spatial Performance of Rail and Road Transportation. In: *The Geography of Transport Systems*. 6th ed. New York, USA, Routledge. https://transportgeography.org/contents/chapter5/rail-transportation-pipelines/rail-road-spatial-performance/.

Tsunashima, H. & Hirose, R. (2022) Condition monitoring of railway track from car-body vibration using time–frequency analysis. *Vehicle System Dynamics*. 60(4), 1170-1187. https://doi.org/10.1080/00423114.2020.1850808.

US High Speed Railway Association. (2025) *Very High Capacity Transportation.* https://ushsr.org/benefits/capacity.html [Accessed 19th October 2025].

Wu, D., & Martín, J. C. (2022) Research on passengers' preference for high-speed railways (HSRs) and high-speed trains (HSTs). *Sustainability*. 14(3), Art. ID 1473. https://doi.org/10.3390/su14031473.

Wu, H., Gong, N., Yang, J. et al. (2024) Investigation of a semi-active suspension system for high-speed trains based on magnetorheological isolator with negative stiffness characteristics. *Mechanical Systems and Signal Processing*. 208, Art. ID 111085. https://doi.org/10.1016/j.ymssp.2023.111085.

Wu, Y., Zeng, J., Shi, H. et al. (2022) A hybrid damping control strategy for high-speed trains running on existing tracks. *Journal of Low Frequency Noise, Vibration and Active Control*. 41(3), 1258-1271. https://doi.org/10.1177/14613484221087513.

Zhao, Y. & Liu, S. (2025). A High-speed Train Operational Risk Prevention and Control Model Based on a Large Language Model. *Studies in Informatics and Control*. 34(3), 63-72. https://doi.org/10.24846/v34i3y202506.

Zhang, H., Ling, L., Zhai, W., & Wang, K. (2024) An active suspension system for enhancing running safety of high-speed trains under strong crosswind. *Proceedings of the Institution of Mechanical Engineers, Part F: Journal of Rail and Rapid Transit*. 238(5), 544-558. https://doi.org/10.1177/09544097231206216.